Two-dimensional analogies to frequency selective surfaces (FSS) on the graphene sheet

Bofeng Zhu[1,2] · Guobin Ren[1,2,*] · Martin J. Cryan [3] · Yixiao Gao[1,2] · Yudong Lian,[1,2] · Jing Wang,[4] · Chenglong Wan,[3] and Shuisheng Jian[1,2]

[1]Key Lab of All Optical Network & Advanced Telecommunication Network of EMC, Beijing Jiaotong University, Beijing 100044, China

[2]Institute of Lightwave Technology, Beijing Jiaotong University, Beijing 100044, China

[3]Department of Electrical and Electronic Engineering, University of Bristol, Bristol, UK

[4]Science and Technology on Optical Radiation Laboratory, Beijing, 100854, China

E-mail: gbren@bjtu.edu.cn

Abstract In this paper we propose that two-dimensional analogies to frequency selective surfaces (FSS) can be achieved on graphene surfaces based on transformation optics. The analogies to representative FSS structures, including the anti-reflecting coating (ARC) and the high-reflecting coating (Bragg reflector) have been investigated through both the analytical Effective Index Method (EIM)/Transfer Matrix Method (TMM) and numerical simulations. Both analytical and numerical solutions have shown that the propagation of plasmons on graphene surface with periodic chemical potentials can be an analogy to the interact of incident light with traditional FSS multilayer dielectric media in which the transmission or reflection can be obtained by EIM/TMM. Combined with the tunability of graphene, the transmission or reflection of plasmons can be tuned by adjusting the bias voltage. The proposed structures and theoretical methods may provide new visions for achieving two-dimensional analogies to traditional structures on graphene.

Keywords: Plasmonics Waveguide · Frequency Selective Surfaces

Introduction

Surface Plasmons are electromagnetic excitations propagating along the interface between a dielectric and a conductor [1]. Graphene is a zero band-gap semiconductor with a two-dimensional form of carbon atoms arranged in the honeycomb lattice [2]. Graphene has an extremely high quantum efficiency for light-matter interactions and supports plasmons with unusual properties [3]. Moreover, the carrier density in graphene can be electrically tuned by over two orders of magnitude through electrical biasing on a field-effect transistor [4] with tuning time below a nanosecond [5]. Recently, transformation optics (TO) has received considerable attention, since it has found an important role in both optical science and engineering fields by offering schemes to control electromagnetic fields [6]. In the view of TO, one graphene sheet can be composed of spatially inhomogeneous or non-uniform conductivity patterns across the surface, which reveals new possibility to manipulate the propagation of graphene plasmons (GPs).

Frequency selective surfaces (FSS) have been developed for spatial filters in microwave and millimeter wave engineering and considered for applications as wireless security, antennas and telecommunications [7]. Although metallic FSS structures work well at microwave frequencies, their applications in the millimeter wave and optical frequency ranges suffer from high power losses and limitations of conducting surface thickness [8]. Thus it is promising to achieve frequency selective functions on a graphene surface, which can be an alternative of FSS on the one-atom-thick platform with comparatively low losses to prevent undesired reflections in the graphene based plasmons circuit.

In this paper we investigate the analogies to two representative FSS structures, including anti-reflecting coating (ARC) and high-reflecting coating (Bragg reflector) on the graphene surface via the Effective Index Method (EIM). Subsequently, reflection from the analogy to an anti-reflecting coating (ARC) on graphene surface are theoretically analyzed by the Transfer Matrix Method (TMM) and verified by numerical solutions. Then transmission and reflection from the analogy to a high-reflecting coating (Bragg reflector) on graphene surface are investigated through theoretical and numerical methods. Finally, we draw the conclusion.

Models and Materials

We first investigate the analogy to an anti-reflection coating (ARC) on graphene based on EIM/TMM theory and numerical simulations. An ARC can ranges from a simple single layer having virtually zero reflectance at just one wavelength, to a multilayer system of more than a dozen layers, having virtually zero reflectance over a broad bandwidth. The simplest ARC is a single layer with quarter wavelength thickness placed between two mediums, targeting a specific zero reflection wavelength by creating destructive interference between the reflections at the interfaces on both sides of the layer [8,9].

As shown in Fig. 1(a), a pattern-free graphene sheet is placed on an uneven doped silicon substrate with a dielectric spacer. The permittivities of the upper space and dielectric spacer are ε_1 and ε_2, respectively. Since the spacer has varied thickness for different regions (h_1, h_2 and h_3 for region L_1, L_2 and L_3), when a bias voltage V_b is applied between graphene and doped silicon, the variation of spacer thickness naturally leads to different chemical potentials on graphene surface (μ_{c1}, μ_{c2} and μ_{c3} respectively). Such design flexibility can be exploited to create regions with different conductivities within a single graphene sheet. Up to now, similar implementations have been widely applied in designing graphene-based waveguide structures [6,10,11].

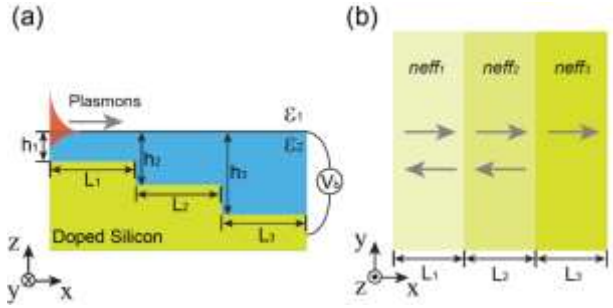

Fig. **1**. Schematic view of the graphene sheet waveguide on an uneven doped silicon substrate with dielectric spacer between them (a) and the equivalent multilayer structure based on the EIM (b). The permittivities in (a) are assumed as ε_1=1 and ε_2=1.76.

According to the Effective Index Method (EIM) [10,12], when GPs encounter regions of graphene with different chemical potentials [Fig. 1(a)], the situation can be treated as the analogy to an incident light propagating within multiple layers composing of two different mediums and one ARC between them [Fig. 1(b)]. Meanwhile, the modal indices of the GPs (*i.e.* $neff_1$, $neff_2$ and $neff_3$) on the graphene above region L_1, L_2 and L_3 in Fig. 1(a) can be regarded as the refractive indexs of three layers in Fig. 1(b). Following by the design rules of ARCs [13], we obtain $neff_2=(neff_1 neff_3)^{1/2}$ and $L_2=\lambda_0/(4neff_2)$, in which λ_0 is the target wavelength and L_2 is middle region length on graphene. In mid-infrared region, the graphene conductivity is modeled via a Drude model with finite temperature correction as [14],

$$\sigma(\omega)=\frac{2e^2}{\pi\hbar}K_{\cdot}T\times\ln\left[2\times\cosh(\frac{\mu_c}{2K_BT})\right]\frac{j}{\omega+j\tau^{-1}} \qquad (1)$$

where j is the imaginary unit, e is the unit electric charge, $\hbar$ is the reduced Planck constant, K_B is the Boltzmann constant, μ_c is the graphene chemical potential, T=300 K is the temperature and ω is the angular frequency. The carrier relaxation time τ can be determined through $\tau = u\mu_c/ev_f^2$, where the Fermi velocity is v_f =10^6 m/s [15], the carrier mobility u =10^4 cm^2/(V·s) is based on the measured data [16] and can be improved by reducing the disorder/impurities of graphene. The surface-normal permittivity of graphene is

assumed as $\varepsilon_{g,n}$=2.5, based on the dielectric constant of graphite [14,17]. By treating the graphene as an ultrathin layer with thickness d=0.34 nm, the tangential permittivity of graphene can be expressed as $\varepsilon_{g,t}$=2.5-i$\sigma(\omega)/\omega\varepsilon_0 d$ [15]. The maximum chemical potential of graphene is set as μ_c=0.72 eV, which can be implemented through electrical biasing [18]. The GPs wavenumbers can be expressed as $\beta \approx j\omega\varepsilon_0(\varepsilon_1+\varepsilon_2)/\sigma(\omega)$ or the following form if Eq. (1) is substituted,

$$\beta \approx \frac{\pi\hbar \quad :_2)}{e^2\mu_c}(1+\frac{j}{\omega\tau})\omega^2. \qquad (2)$$

Here the permittivities are assumed as ε_1=1 and ε_2=1.76 without dispersion and dielectric loss. The indices of GPs on graphene surface above region L_1, L_2 and L_3 can be calculated via $neff=\beta/\beta_0$ ($neff$ can be $neff_1$, $neff_2$ or $neff_3$), where β_0 is the free space wavenumber and β can be obtained through Eq. (2) according to specific chemical potential (μ_{c1}, μ_{c2} or μ_{c3}). All the numerical solutions have been performed by the software package (COMSOL) based on the Finite Element Method (FEM). On the other hand, from Eq. (2) we can see the $\mathrm{Re}(\beta) \propto \mu_c^{-1}$, therefore to satisfy the condition $neff_2 = (neff_1 neff_3)^{1/2}$, we only need to ensure that $\mu_{c2} = (\mu_{c1}\,\mu_{c3})^{1/2}$. The chemical potential can be expressed as $\mu_c = \mathrm{sgn}(n)\hbar v_f(\pi|n|)^{1/2}$, in which n is the bias induced carrier density. According to the parallel-plate capacitor model [10], we have $n = -\varepsilon_0\varepsilon_2 V_b/eh$, in which V_b is the bias voltage, h is the dielectric spacer thickness. And therefore one has the following relationships, $\mu_c \propto (V_b/h)^{1/2}$ and $neff \propto (h/V_b)^{1/2}$ according to Eq. (2). Once the dielectric spacer thicknesses of the three regions h_1, h_2 and h_3 fulfill the relation $(h_2)^2 = h_1 h_3$, the anti-reflection condition can be satisfied under any bias voltage, providing possibility to control the target wavelength λ_0 via electrical biasing.

Numerical Simulations and Theoretical Analysis

The transfer matrix method (TMM) is a simple approach to model waves passing through multiple layers [9]. This method employs continuity boundary conditions between dielectric layers and wave equations to describe reflection or transmission across each layer. Then, if the electric field is known at the beginning of one layer, a transfer matrix based on the wave equation can be used to determine the electric field at the other end of the layer [8,19]. Compared with other methods adopted in analyzing FSS multilayer structures, such as Time-Based Optical Modeling Methods (*e.g.* FDTD) or Rigorous Coupled Wave Analysis (RCWA), the TMM owes the fastest computation speed with satisfactory accuracy [9]. More detailed information about the TMM we adopt in this paper can be found in [20].

We first focus on the graphene sheet with three different but fixed chemical potentials (due to single bias voltage V_b) and alter the length of the middle region L_2. The reflection spectrum by EIM/TMM and numerical solutions are shown in Fig. 2(a). For simplicity, the lengths of the first and last region are fixed at L_1=L_3=100 nm where the plasmon attenuation has been taken into account. The chemical potentials of the three regions are respectively μ_{c1}=0.72 eV, μ_{c2}=0.6 eV and μ_{c3}=0.5 eV in Fig. 2(a). We choose three target anti-reflection wavelengths λ_0=6.5 μm, 7 μm and 7.5 μm by altering middle region length as L_2=54 nm, 63 nm and 72 nm, respectively. The incident wavelength spans from λ=6 μm to 8 μm.

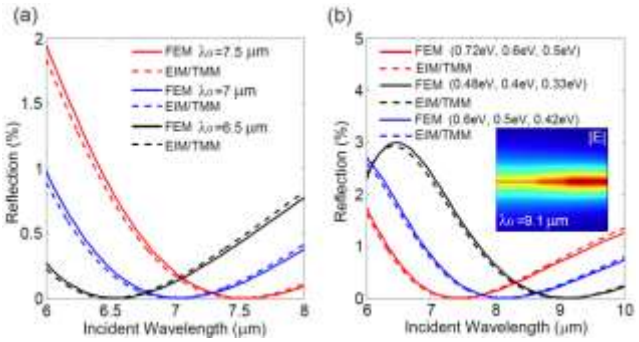

Fig. 2. Dependencies of the reflectance for the analogy to an anti-reflection coating (ARC) on wavelength with various target anti-reflection wavelengths λ_0 (a) and chemical potentials (b) by numerical solutions (solid lines) and EIM/TMM (dashed lines). Shown in the inset of (b) is the normalized electric field $|E|$ profile on xz plane

on the target wavelength (λ_0=9.1 μm).

As rendered in Fig. 2(a), the reflectance reaches near zero at the target anti-reflection wavelength. Furthermore, the analytical results derived from EIM/TMM agree very well with numerical FEM solutions, implying that the EIM/TMM can be applied in the design of analogies to traditional FSS structures. Although the target wavelength λ_0 can be altered by changing the region length L_2, it is unrealistic in the practical applications once the substrate structure is fabricated. Therefore we discuss the situation in which length L_2 is fixed while different bias voltages V_b are adopted and consequently, the chemical potentials of three regions would alter simultaneously. Here various groups of chemical potentials are used to represent different bias voltages with dielectric spacer thicknesses are assumed to fulfill anti-reflection conditions $(h_2)^2=h_1h_3$, and therefore in each group, chemical potentials satisfy $(\mu_{c2})^2=\mu_{c1}\mu_{c3}$. The results derived from EIM/TMM and numerical solutions are presented in Fig. 2(b). The incident wavelength spans from λ=6 μm to 10 μm with middle region length is L_2=70 nm. In Fig. 2(b), the reflection spectrum shifts to the short wavelength as the chemical potentials increase (the bias voltage V_b increases), which can be explained by considering the $neff_2$ decreases as the μ_{c2} increases [see Eq.(2)], causing the blue shift of the anti-reflection wavelength λ_0. Meanwhile, the bias voltage V_b enables a tunable reflection spectrum, endowing the analogy to ARC with flexibility in practical applications.

We next investigate the analogy to high-reflection coating on the graphene surface via EIM/TMM theory and numerical simulations. Generally, a high-reflection coating in FSS is composed of multilayer dielectric mediums with periodic high/low refractive indexs. Recently, a graphene-coated dielectric grating system has been proposed and shown potential in several applications, such as waveguiding [21], active slow graphene plasmons [22] and Bragg reflectors [17]. As presented in the previous study [17], the high Bragg reflection can be realized by alternatively stacking graphene–silicon and graphene–air waveguides.

Nevertheless, several issues need to be investigated further. Firstly, the chemical potential of graphene sheet was previously assumed to be uniform. In fact, it should be more realistic to focus on one graphene sheet with non-uniform chemical potentials, which can be naturally introduced under single bias voltage between graphene sheet and uneven dielectric substrate (dielectric gratings). Secondly, the transmission spectrum of the proposed Bragg reflector was calculated through FDTD simulations, which could be time-consuming and hampered by the limited computational resources. As is rendered before, the EIM/TMM provides the fastest calculation speed, physical insight as well as satisfactory consistency to rigorous numerical simulations.

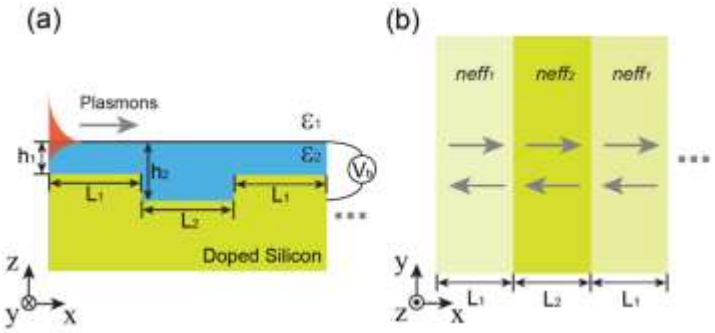

Fig. **3**. (a) Schematic view of graphene sheet waveguide on the uneven doped silicon substrate with dielectric spacer between them (only show one and a half periods). (b) The equivalent Bragg reflector based on multilayer dielectric structure by EIM.

We subsequently focus on the plasmons propagating on graphene sheet with periodically alternated chemical potentials, which can be regarded as the analogy to high-reflection coating consisting of multilayer dielectric materials with periodic high/low refractive indexs. Figure 3 illustrates the schematics under consideration (only show one and a half periods). Each period is composed of two regions with lengths L_1 and L_2 and chemical potentials μ_{c1} and μ_{c2}, which are naturally introduced by the distinct spacer thickness h_1 and h_2 under single bias voltage V_b, supporting plasmons with modal indices $neff_1$ and $neff_2$. According to the EIM, the modal indices $neff_1$ and $neff_2$ on graphene regions L_1 and L_2 in Fig. 3(a) can be regarded as the refractive indexs of two mediums in Fig. 3(b). We subsequently present the transmission

spectra with various number of periods (N) in Fig. 4(a) and chemical potentials (μ_c) in Fig. 4(b) through analytical and numerical methods. For better presentation, in Fig. 4(a), the reflection spectrum for N=9 and snapshots of the normalized field $|E|$ for two different wavelengths are shown as well. The chemical potentials in one period are set as μ_{c1}=0.4 eV and μ_{c2}=0.6 eV in Fig. 4(a), with corresponding lengths L_1=L_2=60 nm. In Fig. 4(b), various groups of chemical potential represent different implemented bias voltages. The wavelength spans from λ= 6 μm to 10 μm..

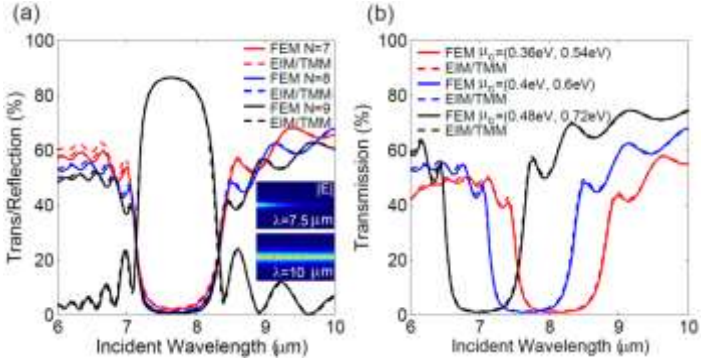

Fig. 4. Dependencies of transmission and reflection of the analogy to high-reflection coating (Bragg reflector) on number of periods N (a) and chemical potential μ_c (b) by numerical solutions (solid lines) and EIM/TMM (dashed lines). Shown in the inset are the normalized electric field $|E|$ profiles on xz plane for N=9 on the two wavelengths (λ=7.5 μm and λ=10 μm).

As shown in the figure, the transmission and reflection of the analogy to Bragg reflector can be well described by EIM/TMM. The slight disagreement at short wavelengths can be attributed to the scattering losses due to the discontinuities between two adjacent regions. Figure 4(a) shows that larger number of periods results in lower transmission near the Bragg wavelength (where reflectance can be as high as 83%). Meanwhile, in Fig. 4(b), higher chemical potential (or higher V_b) gives rise to the blue shift of Bragg wavelength and higher transmission. The aim of this paper is to analyze traditional FSS structures and their two-dimensional analogies on graphene, which is different to the previous study [22] in which the aim was to control and slow down the group velocity of plasmons. Meanwhile, we adopt the EIM/TMM based model, which has been commonly applied in the design of traditional FSS structures. We show that such model ensures fast computation speed, high accuracy and therefore has potential in the future design of analogous FSS structure on graphene surface.

Conclusions

In this paper, we analyze the two-dimensional analogies to representative frequency selective surfaces structures, namely the anti-reflecting coating and the high-reflecting coating (Bragg reflector) on graphene. As graphene plasmons propagate on the graphene surface with spatially alternated chemical potentials, such a case can be treated as an analogy to incident light interacting with traditional FSS structure composing of multilayer dielectric mediums. The corresponding reflection or transmission can be obtained by the Effective Index Method /Transfer Matrix Method, which has shown good agreement with rigorous numerical solutions. The reflection or transmission can be tuned dynamically by adjusting a single bias voltage on graphene. The proposed structures and procedures may provide new directions to achieve two-dimensional analogies to traditional structures on graphene.

Acknowledgements

This work was supported by the Fundamental Research Funds for the Central Universities (Grant No. 2015YJS016).

References

1. Maier SA (2007) Plasmonics: Fundamentals and Applications. Springer, New York

2. Novoselov KS, Geim AK, Morozov SV, Jiang D, Katsnelson MI, Grigorieva IV, Dubonos SV, Firsov AA (2005) Two-dimensional gas of massless Dirac fermions in graphene. Nature 438 (7065):197-200. doi:10.1038/nature04233
3. Grigorenko AN, Polini M, Novoselov KS (2012) Graphene plasmonics. Nature Photonics 6 (11):749-758. doi:10.1038/nphoton.2012.262
4. Ju L, Geng B, Horng J, Girit C, Martin M, Hao Z, Bechtel HA, Liang X, Zettl A, Shen YR, Wang F (2011) Graphene plasmonics for tunable terahertz metamaterials. Nature nanotechnology 6 (10):630-634. doi:10.1038/nnano.2011.146
5. Liu M, Yin X, Ulin-Avila E, Geng B, Zentgraf T, Ju L, Wang F, Zhang X (2011) A graphene-based broadband optical modulator. Nature 474 (7349):64-67. doi:10.1038/nature10067
6. Vakil A, Engheta N (2011) Transformation optics using graphene. Science 332 (6035):1291-1294. doi:10.1126/science.1202691
7. Kiani GI, Ford KL, Esselle KP, Weily AR, Panagamuwa CJ (2007) Oblique Incidence Performance of a Novel Frequency Selective Surface Absorber. IEEE Transactions on Antennas and Propagation 55 (10):2931-2934. doi:10.1109/tap.2007.905980
8. Oraizi H, Afsahi M (2007) Analysis of planar dielectric multilayers as FSS by transmission line transfer matrix method (TLTMM). Progress In Electromagnetics Research, PIER 74:217-240
9. Han K, Chang C-H (2014) Numerical Modeling of Sub-Wavelength Anti-Reflective Structures for Solar Module Applications. Nanomaterials 4 (1):87-128. doi:10.3390/nano4010087
10. Zheng J, Yu L, He S, Dai D (2015) Tunable pattern-free graphene nanoplasmonic waveguides on trenched silicon substrate. Scientific reports 5:7987. doi:10.1038/srep07987
11. Zhu B, Ren G, Gao Y, Yang Y, Wu B, Lian Y, Wang J, Jian S (2014) Spatial Splitting and Coupling of the Edge Modes in the Graphene Bend Waveguide. Plasmonics. doi:10.1007/s11468-014-9861-6
12. Xu W, Zhu ZH, Liu K, Zhang JF, Yuan XD, Lu QS, Qin SQ (2015) Dielectric loaded graphene plasmon waveguide. Optics express 23 (4):5147-5153. doi:10.1364/oe.23.005147
13. H.A.Macleod (1986) Thin-Film Optical Filters. Institute of Physics Publishing,
14. Falkovsky LA (2008) Optical properties of graphene and IV–VI semiconductors. Physics-Uspekhi 51 (9):887-897. doi:10.1070/PU2008v051n09ABEH006625
15. Gao W, Shu J, Qiu C, Xu Q (2012) Excitation of plasmonic waves in graphene by guided-mode resonances. ACS nano 6 (9):7806-7813. doi:10.1021/nn301888e
16. Novoselov KS, Geim AK, Morozov SV, Jiang D, Zhang Y, Dubonos SV, Grigorieva IV, Firsov AA (2004) Electric field effect in atomically thin carbon films. Science 306 (5696):666-669. doi:10.1126/science.1102896
17. Tao J, Yu X, Hu B, Dubrovkin A, Wang QJ (2014) Graphene-based tunable plasmonic Bragg reflector with a broad bandwidth. Optics letters 39 (2):271-274. doi:10.1364/OL.39.000271
18. Gomez-Diaz JS, Perruisseau-Carrier J (2013) Graphene-based plasmonic switches at near infrared frequencies. Optics express 21 (13):15490-15504. doi:10.1364/OE.21.015490
19. Hecht E, Ganesan A (2002) Optics. Pearson Education, San Francisco, CA, USA
20. Junesch J, Sannomiya T, Dahlin AB (2012) Optical properties of nanohole arrays in metal-dielectric double films prepared by mask-on-metal colloidal lithography. ACS nano 6 (11):10405-10415. doi:10.1021/nn304662e
21. Kong XT, Bai B, Dai Q (2015) Graphene plasmon propagation on corrugated silicon substrates. Optics letters 40 (1):1-4. doi:10.1364/OL.40.000001
22. Lu H, Zeng C, Zhang Q, Liu X, Hossain MM, Reineck P, Gu M (2015) Graphene-based active slow surface plasmon polaritons. Scientific reports 5:8443. doi:10.1038/srep08443